Field-Induced and Thermal Electron Currents from Earthed Spherical Emitters

J. T. Holgate* and M. Coppins

Blackett Laboratory, Imperial College London, London SW7 2BW, United Kingdom

(Received 17 October 2016; revised manuscript received 3 March 2017; published 24 April 2017)

The theories of electron emission from planar surfaces are well understood, but they are not suitable for describing emission from spherical surfaces; their incorrect application to highly curved, nanometer-scale surfaces can overestimate the emitted current by several orders of magnitude. This inaccuracy is of particular concern for describing modern nanoscale electron sources, which continue to be modeled using the planar equations. In this paper, the field-induced and thermal currents are treated in a unified way to produce Fowler-Nordheim-type and Richardson-Schottky-type equations for the emitted current density from earthed nanoscale spherical surfaces. The limits of applicability of these derived expressions are considered along with the energy spectra of the emitted electrons. Within the relevant limits of validity, these equations are shown to reproduce the results of precise numerical calculations of the emitted current densities. The methods used here are adaptable to other one-dimensional emission problems.

DOI: 10.1103/PhysRevApplied.7.044019

I. INTRODUCTION

The emission of electrons from the surface of a material is a well-known quantum phenomenon which has found a vast number of technological uses; applications such as field-emission displays, thermoelectric generators, photomultipliers, electron microscopes, and electron guns are just a few examples of technologies which are reliant upon electron emission. It is, therefore, unsurprising that electron emission has attracted considerable research interest over the past century.

The emitted current is dependent upon the temperature of the material and the electric-field strength at its surface. At high temperatures, the hot electrons can escape from the material; this process is called thermal emission and, for a flat surface, the theoretical emitted current density is

$$J_{\mathrm{RS}} = \lambda^T A_R T^2 \exp\left\{\frac{-1}{k_B T}\left[\phi - \left(\frac{e^3 F}{4\pi\epsilon_0}\right)^{1/2}\right]\right\}, \quad (1)$$

where T is the temperature of the emitter, F is the electric-field strength at the emitting surface, ϕ is the average amount of energy needed to remove an electron from the material when no field is applied, known as the work function, and A_R is Richardson's constant. Boltzmann's constant, the electron charge, and the permittivity of free space are represented by k_B, e, and ϵ_0 respectively. The material-specific factor λ^T accounts for effects such as electron reflection and scattering; a good discussion of the difficulties involved in calculating its precise value is provided by Modinos [1]. Equation (1) is generally known as the classical Richardson-Schottky (RS) equation when $\lambda^T = 1$. If, additionally, $F = 0$, then the classical RS equation reduces to the classical Richardson equation [2,3]. The extension to relatively weak electric fields was originally due to Schottky [4].

In the opposite limit of high electric fields and low temperatures, electrons are extracted from the surface in a process known as field-induced, or simply field, emission. The emitted current density in this case is given by

$$J_{\mathrm{FN}} = \frac{\lambda^F a_{\mathrm{FN}} F^2}{\phi}\exp\left(\frac{-\nu_F b_{\mathrm{FN}}\phi^{3/2}}{F}\right), \quad (2)$$

where a_{FN} and b_{FN} are the universal Fowler-Nordheim constants [5] and the factors λ^F and ν_F depend on the specific emitting surface and material. Equation (2) is known as the classical Fowler-Nordheim (FN) equation when λ^F and ν_F take the values given by a perfectly conducting planar emitter [6–9].

These two emission processes are special cases of the same emission phenomenon; the first theory of unified thermal and field-induced electron emission from planar surfaces was provided by Murphy and Good [9]. That work identified two main emission regimes, where either the classical RS or FN equation applies, separated by a transition region. Compound expressions for the emitted current density from planar surfaces in the transition region were found by Christov [10] and, more recently, by Jensen [11], who also included photoinduced emission in his general field-thermal (GFT) theory.

These investigations have been relatively successful at describing electron emission from flat surfaces, but studies from the 1990s demonstrated that the classical FN equation is inaccurate for emitters smaller than 10–20 nm [12–14]. The tips of emitting surfaces have now reached radii of curvature smaller than 5 nm [15,16], but the planar FN equation continues to used for the analysis of experimental

*j.holgate14@imperial.ac.uk

data [17,18]. The inaccuracy of the classical FN equation for these nanoscale emitters has prompted the development of spherical FN-type equations [19,20] and a spherical generalization of Jensen's GFT theory [21], although the series expansions used in the latter work become unsatisfactory for very small ($\lesssim$5 nm) spheres.

In this paper, the methodology of Murphy and Good is applied in order to produce RS-type and FN-type equations for the emitted current density from small earthed spherical emitters and to define, in T-F parameter space, the regimes where these equations are valid. The energy distributions of the emitted electrons in each emission regime are also considered. The results derived here are of general applicability. However, where required, the properties of tungsten are used to produce specific plots and examples. Tungsten is an example of a near-ideal emitter, with a work function of 4.5 eV and a Fermi energy of 6 eV [1], and it is often used in commercial applications of electron emission. Temperatures above the melting point of tungsten are used in some examples and are relevant to liquid-metal emitters [22].

II. BASIC EQUATIONS

The simplest description of electrons in a metallic material is the free-electron theory. This theory assumes that electrons in the material behave as free particles with their total energies E, as measured from the base of the conduction band, given by the Fermi-Dirac distribution function,

$$f_{\mathrm{FD}}(E,T)=\frac{1}{1+\exp[(E-E_F)/k_BT]}, \tag{3}$$

where T is the thermodynamic temperature of the metal. The Fermi energy, E_F, is defined as the total electron energy of the state for which the occupation probability is 0.5. The free-electron theory fails to account for the internal atomic structure—and hence the existence of a band gap—in solids, but it remains an excellent first approximation for the electron energy distribution; for liquids, there is much less internal atomic structure and the free-electron theory should be an even better approximation [23]. The following analysis assumes the electron gas to be in thermodynamic equilibrium and hence to obey Fermi-Dirac statistics.

The total energy of an electron in the free-electron gas, defined above as E, can be split into the kinetic energy associated with the components of velocity parallel to and normal to the emitter surface, which are denoted as E_p and W, respectively. The contribution to the electron current density incident on the inside of the emitting surface due to electrons with energy components between W and $W+dW$ and E_p and E_p+dE_p is given by

$$\begin{aligned} d^2Z &= z_s f_{\mathrm{FD}}(W,E_p,T)dE_p dW \\ &= \frac{z_s dE_p dW}{1+\exp[(W+E_p-E_F)/k_BT]}, \end{aligned} \tag{4}$$

as deduced from the formulas in Ref. [24]. The Sommerfeld supply density z_s is a universal constant with the value $z_s \approx 1.618311\times10^{14}\ \mathrm{A\,m^{-2}\,eV^{-2}}$ [5].

When an electron is incident on the material surface, it may either be reflected, so that it remains within the material, or transmitted, in which case it escapes and contributes to the emitted current density. The probability that an electron crosses the surface barrier is given by the transmission coefficient $D(W,F)$, which is a function of the electric field at the surface, F, and the normal component of energy only. F is defined to be positive when the surface is negatively charged, as is the case for all of the emitters considered here. It follows that the total emission current density is given by

$$\begin{aligned} J(F,T) &= \int_0^\infty \left[z_s \int_0^\infty f_{\mathrm{FD}}(W,E_p,T)dE_p \right] D(W,F)dW \\ &= \int_0^\infty N(W,T)D(W,F)dW, \end{aligned} \tag{5}$$

where the current-density supply function $N(W,T)$, i.e., the incident electron current density per unit normal energy range, is

$$\begin{aligned} N(W,T) &= z_s \int_0^\infty \frac{1}{1+\exp[(E-E_F)/k_BT]}dE_p \\ &= -z_s k_B T\left[\ln\left(1+\exp\left(-\frac{W+E_p-E_F}{k_BT}\right)\right)\right]_0^\infty \\ &= z_s k_B T \ln\left(1+\exp\left(-\frac{W-E_F}{k_BT}\right)\right). \end{aligned} \tag{6}$$

Two shortcomings of the free-electron theory, and hence this form of $N(W,T)$, should be noted. First, it is valid only for metallic emitters, as the band structure in narrow-gap semiconductors and few-layer graphene leads to anisotropic distributions of electrons [25] and the electrons in single-layer graphene are described by the 2D, rather than the 3D, Fermi-Dirac distribution [26]. Second, the physical shape and size of the emitter can lead to quantum confinement effects, such as those studied by Qin *et al.* for nanowall emitters [27] and by Patterson and Akinwande for nanoscale wire emitters [28], which indicate that Eq. (6) is unsuitable for emitters smaller than 2 nm. Nevertheless, it is assumed here that Eq. (6) provides an adequate description of the supply function and that differences between the planar and spherical theories are due solely to the differences in the external electric potential.

The material surface is described by a one-dimensional potential-energy barrier denoted by $U(z)$, where z is in the direction normal to the surface. The probability that an electron can traverse this barrier is given by $D(W,T)$. A generalized semiclassical quantum-mechanical approximation for $D(W,T)$ was proposed by Miller and Good [29] and leads to the same formula as a slightly different, and

much earlier, approach by Kemble [30]. This formula may be written as

$$D(W,F) = \{1 + \exp[G(W,F)]\}^{-1}, \tag{7}$$

$$G(W,F) = g_e \int_{z_1}^{z_2} M^{1/2}(z)dz, \tag{8}$$

$$M(z) = U(z) - W, \tag{9}$$

where $g_e \approx 10.24633\ \mathrm{eV}^{-1/2}\ \mathrm{nm}^{-1}$ is the Jeffreys-Wentzel-Kramers-Brillouin (JWKB) constant for an electron; in terms of fundamental constants, $g_e = (8m)^{1/2}/\hbar$, where m is the electron mass and $\hbar$ the reduced Planck constant [5]. The electron motive energy $M(z)$ defines the form of the tunneling barrier, as given in the next section for the planar and spherical cases, while the values of z_1 and z_2 are the roots of $M(z) = 0$. These roots may be either purely real, in which case the normal energy W is below the peak of the barrier and the roots are chosen such that $z_1 < z_2$, or complex conjugates, in which case z_1 is selected to have a positive imaginary part and z_2 to have a negative imaginary part. As such, this form of $D(W,F)$ can account for both tunneling through a barrier and scattering above it. This approximation fails for large values of W, above a limiting value W_l, which cause the real parts of z_1 and z_2 to approach the singularity in $M^2(z) = 0$ at $z = 0$. Fortunately, $D(W,F)$ is well approximated as 1 when $W > W_l$.

The transmission coefficient clearly depends on the form of the barrier potential function $U(z)$, which is different for spherical and planar surfaces. For a planar conducting surface with an applied electric field F, this function is given by [1]

$$U_p(z) = \begin{cases} 0, & \text{for } z < z_c \\ E_F + \phi - \frac{c_s^2}{4ez} - eFz, & \text{for } z > z_c \end{cases}, \tag{10}$$

where ϕ is the work function of the material, which is the amount of energy required by an electron to escape the surface at zero temperature when no field is applied, and $c_s = (e^3/4\pi\epsilon_0)^{1/2} \approx 1.199985\ \mathrm{eV\,(V/nm)}^{-1/2}$ is the Schottky constant [5]. The term containing c_s is attributable to the image force on an electron near a conducting planar surface, while the last term is attributable to the applied field. The point z_c is given by the position larger than $z = 0$ where the potential barrier drops to zero, so that the singularity at $z = 0$ is avoided. This potential barrier is plotted as the thick blue line in Fig. 1 for $F = 3\ \mathrm{V\,nm}^{-1}$.

The potential barrier of an earthed spherical surface is given by [19]

$$U_s(r) = \begin{cases} 0, & \text{for } r < r_c \\ E_F + \phi - \frac{c_s^2 a}{2e(r^2 - a^2)} & \\ -eFa\left(1 - \frac{a}{r}\right), & \text{for } r > r_c \end{cases}, \tag{11}$$

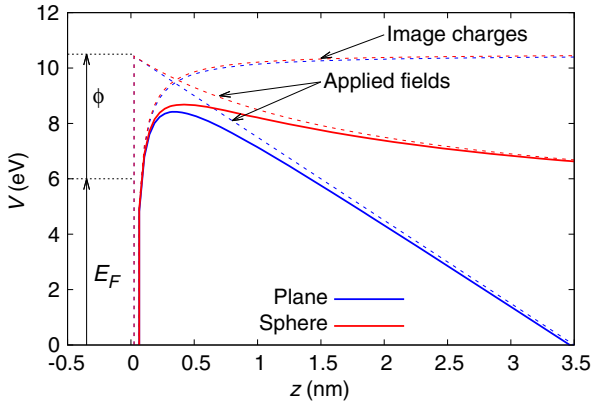

FIG. 1. The planar and spherical potential-energy barriers for $E_F = 6$ eV, $\phi = 4.5$ eV, $F = 3\ \mathrm{V\,nm}^{-1}$, and $a = 2$ nm. The individual contributions from the image charge and the applied field terms are shown by the dashed lines.

where r is the radial distance from the center of the sphere, a is the radius of the sphere, and r_c is the radius, slightly larger than a, at which the potential barrier drops to zero. The field F at the emitter surface is repulsive to electrons in all of the cases considered here, as positively charged spheres may accumulate a negative charge cloud which complicates the problem. The spherical barrier tends to the planar barrier for large spheres; this may be seen by substituting $r = z + a$ and allowing $a \to \infty$ in order to obtain Eq. (10). This potential barrier is illustrated, as a function of $z = r - a$, by the thick red curve in Fig. 1. The spherical barrier is always higher and wider than the planar barrier for a given value of F, so it will produce a smaller emitted current. The quantification of this difference between the spherical and the planar barrier is the principal focus of this paper.

It is worth mentioning briefly that Jensen *et al.* have recently given an expression for the electrostatic potential due to the image charge of a sphere equivalent to $-c_s^2 a/e(r^2 - a^2)$ [31]. However, in the limit $a \to \infty$, this is a factor of 2 away from the correct expression for the planar case. This discrepancy seems to arise from the use of the formula for the Coulomb potential. The Coulomb potential is not applicable to image charges because work must be done on the real charge only—not the image charge—as opposed to a system of two point charges, where work must be done on both (see Sec. 3.2.3 of Ref. [32]). This effect accounts for the erroneous factor of 2.

Having obtained convenient expressions for the supply function and transmission coefficient for both the spherical and planar cases, the emitted current density follows simply from Eq. (5). This integral can be evaluated approximately in the field-related and thermally related limits to give the FN-type and RS-type equations for emission from planar or spherical surfaces. Before doing so, the problem is reformulated in terms of dimensionless parameters and functions which are consistent with existing emission theories.

III. FORMALISM IN TERMS OF y AND A

The basic equations of the previous section can be expressed in terms of dimensionless parameters in order to reduce the number of dependent variables and to simplify the derivations of the FN-type and RS-type equations. These new parameters are the Nordheim parameter

$$y = \frac{c_s F^{1/2}}{H}, \tag{12}$$

where $H = E_F + \phi - W$ is the zero-field barrier height, and the size parameter is

$$A = \frac{eaF^{1/2}}{c_s}, \tag{13}$$

where $e/c_s \approx 0.8333436\ \mathrm{nm}^{-1}\,(\mathrm{V/nm})^{-1/2}$. The variable A, although mathematically convenient, is an obscure measure of the physical size of the spherical emitter, so, while the theory is developed in terms of A, specific examples are given in terms of a. This choice of A is designed to make it independent of H, which simplifies the series expansions made in the following sections, but it is noted that the alternative size parameter ϕ/eFa was employed by Kyritsakis and Xanthakis in their work on field-induced emission from earthed spheres [20].

Equations (8) and (9) can be rewritten in terms of y and A as

$$G(W,F) = b_{\mathrm{FN}}\frac{H^{3/2}}{F}v^*(y,A), \tag{14}$$

where

$$b_{\mathrm{FN}} = \frac{2g_e}{3e} \approx 6.830890\ (\mathrm{eV})^{-3/2}\,\mathrm{V\,nm}^{-1} \tag{15}$$

is the second FN constant [5] and $v^*(y,A)$ is called the barrier-form correction factor. This function is denoted v^*, rather than simply v, in order to distinguish it from the principal Schottky-Nordheim barrier function, which describes emission through the planar barrier given by Eq. (10). The function $v^*(y,A)$ becomes $v(y)$ in the planar limit. Utilizing the integration variable $\rho = r/a$ gives, for the spherical potential in Eq. (11),

$$v^*(y,A) = \frac{3}{2}Ay\int_{\rho_1}^{\rho_2}\left[1 - \frac{y}{2A(\rho^2-1)} - Ay\left(1-\frac{1}{\rho}\right)\right]^{1/2}d\rho. \tag{16}$$

The integration limits ρ_1 and ρ_2 are given by the roots of $M(\rho) = 0$, which, in this case, are the two solutions of the cubic equation

$$(Ay-1)\rho^3 - Ay\rho^2 + \left(1 + \frac{y}{2A} - Ay\right)\rho + Ay = 0 \tag{17}$$

that are greater than 1. When finding the emitted current, it is much easier to refer to approximate formulas or tabulated values of $v^*(y,A)$, as provided in the Appendix along with a least-squares functional fit, than to numerically evaluate this integral on a case-by-case basis.

The parameter y and the concept of a barrier-form correction factor were introduced by Nordheim [6], but the mathematical function and values he derived for the planar case were subsequently found to be incorrect. Correct values for the correction function $v(y)$ for the planar case were tabulated by Burgess *et al.* [8]. This notation was subsequently used by Murphy and Good in their unified approach to thermal and field-induced emission [9], which forms the basis of the spherical theory developed here. The planar equivalent of Eq. (16) corresponds to the large-A limit of the spherical case and, as shown in the Appendix, letting $A \to \infty$ yields the values calculated by Burgess *et al.*

Much more recently, Forbes and Deane discovered an approximate formula for the planar barrier-form correction factor

$$v(y) \approx 1 - y^2 + \frac{y^2\ln y}{3}, \tag{18}$$

which gives an error not greater than 0.33% over the range $0 < y \le 1$ [33,34]. This formula was extended to the earthed spherical barrier-form correction factor by Kyritsakis and Xanthakis, who gave a formula equivalent to [20]

$$v^*(y,A) \approx 1 - y^2 + \frac{y^2\ln y}{3} + \frac{1}{yA}\left(\frac{4}{5} - \frac{7y^2}{40} - \frac{y^2\ln y}{100}\right), \tag{19}$$

where terms on the order of $(yA)^{-2}$ and higher were neglected. This formula is plotted in Fig. 2 as a function of y for various values of A and compared to the numerical solution of Eq. (16). Figure 2 shows Eq. (19) to be an excellent approximation over the expected range of validity $yA \gg 1$.

The series expansions made in the following sections require the introduction of the second barrier-form correction function,

$$t^*(y,A) = v^*(y,A) - \frac{2y}{3}\frac{\partial v^*(y,A)}{\partial y}. \tag{20}$$

Following Forbes and Deane's derivation of an accurate formula for the planar case [33,34], Kyritsakis and Xanthakis also produced the approximate formula [20]

$$t^*(y,A) \approx 1 + \frac{y^2}{9} - \frac{y^2\ln y}{11} + \frac{1}{yA}\left(\frac{4}{3} - \frac{y^2}{500} - \frac{y^2\ln y}{15}\right), \tag{21}$$

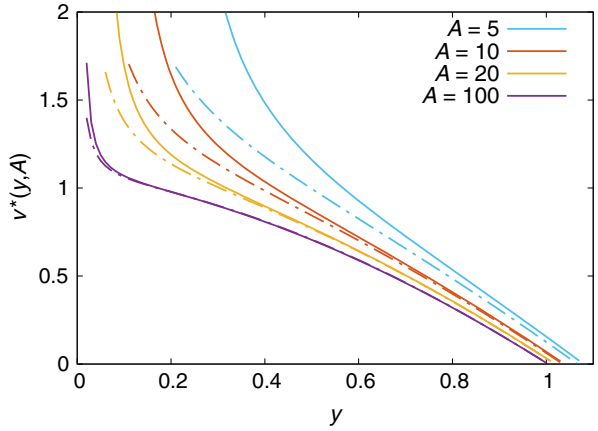

FIG. 2. Comparison of the exact evaluation of the barrier-form correction factor [Eq. (16), solid lines] to the approximate formula from Ref. [20] [Eq. (19), dotted-dashed lines].

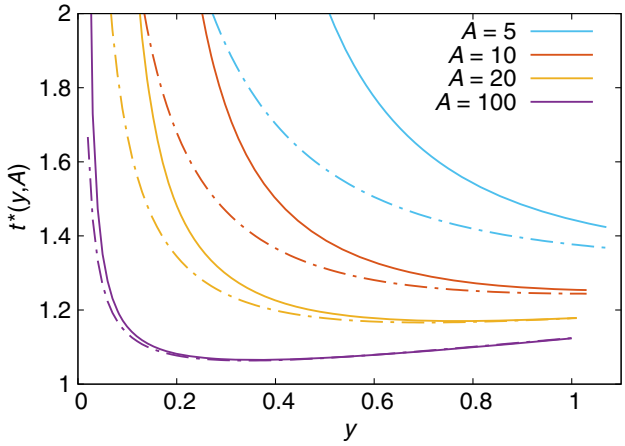

FIG. 3. Comparison of the exact evaluation of the second barrier-form correction factor [Eq. (20), solid lines] to the approximate formula from Ref. [20] [Eq. (21), dotted-dashed lines].

where terms on the order of $(yA)^{-2}$ and above have again been excluded. Figure 3 shows a comparison of this approximate formula to the exact numerical solution; again, Eq. (21) is shown to be accurate over the expected range of validity $yA \gg 1$.

IV. FIELD-INDUCED EMISSION

Emission in the low-temperature, high-field regime, often referred to as the cold-field-emission regime in the field-emission literature [5,35], is dominated by electrons with energies close to the Fermi energy, $W \approx E_F$, which is well below the barrier peak. Each electron, therefore, has a very small probability of tunneling through the barrier, so the approximation $G(W,F) \gg 1$, and hence

$$D(W,F) \approx \exp[-G(W,F)], \tag{22}$$

can be made. Equation 22 is the simple JWKB-type formula [36]. The integral in Eq. (5) can be put into an analytical form by retaining only the first two terms in a power-series expansion of $G(W,F)$ about the Fermi energy. This expansion,

$$-G(W,F) = -b + c(W-E_F) - f(W-E_F)^2 + \cdots, \tag{23}$$

has the coefficients

$$b = G(W=E_F,F) = b_{\mathrm{FN}}\frac{\phi^{3/2}}{F}v^*(y_0,A), \tag{24}$$

$$c = \left.\frac{dG(W,F)}{dW}\right|_{W=E_F} = \frac{3b_{\mathrm{FN}}}{2}\frac{\phi^{1/2}}{F}t^*(y_0,A), \tag{25}$$

$$f = \frac{1}{2}\left.\frac{d^2G(W,F)}{dW^2}\right|_{W=E_F} = \frac{3b_{\mathrm{FN}}}{8}\frac{1}{F\phi^{1/2}}u^*(y_0,A), \tag{26}$$

where b_{FN} is given by Eq. (15) and y_0 is the value of y at $W = E_F$,

$$y_0 = \frac{c_s F^{1/2}}{\phi}. \tag{27}$$

The barrier-form correction functions $v^*(y,A)$ and $t^*(y,A)$ are given by Eqs. (16) and (20), while the additional function $u^*(y,A)$ is defined as

$$u^*(y,A) = t^*(y,A) - 2y\frac{\partial t^*(y,A)}{\partial y}. \tag{28}$$

The straightforward generalization of Murphy and Good's series expansion to the spherical case is due to A's being independent of H, and hence W, so that $\partial A/\partial W$ need not be considered. With these approximations made, Eq. (5) becomes

$$\begin{aligned} J(F,T) = {} & z_s k_B T \exp(-b) \\ & \times \int_0^\infty \exp[c(W-E_F)] \\ & \times \ln\left[1+\exp\left(-\frac{W-E_F}{k_B T}\right)\right] dW. \end{aligned} \tag{29}$$

The value of the integrand drops off rapidly as W departs from E_F, so the lower integration limit can be taken as $-\infty$, and the use of an integration variable $\nu = \exp[(W-E_F)/k_B T]$ yields the standard form

$$J(F,T) = \frac{z_s k_B T}{c}\exp(-b)\int_0^\infty \frac{\nu^{(ck_BT-1)}}{1+\nu}d\nu. \tag{30}$$

This integral converges, provided that $ck_BT < 1$, to give the field-induced emitted current density J_T at nonzero temperatures as

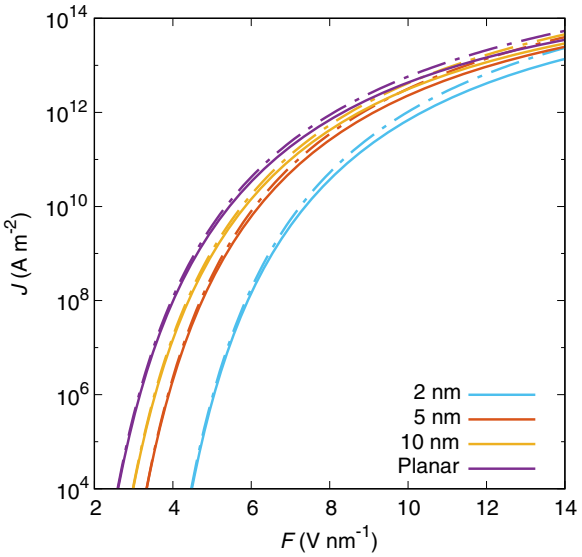

FIG. 4. Field-induced current densities from surfaces with $\phi = 4.5$ eV at $T = 300$ K, as calculated using the zero-temperature FN-type equation for a spherical emitter, i.e., Eq. (33) with correction factors given by Eqs. (A2) and (A7) (dotted-dashed lines) and the precise numerical evaluation of Eq. (5) (solid lines).

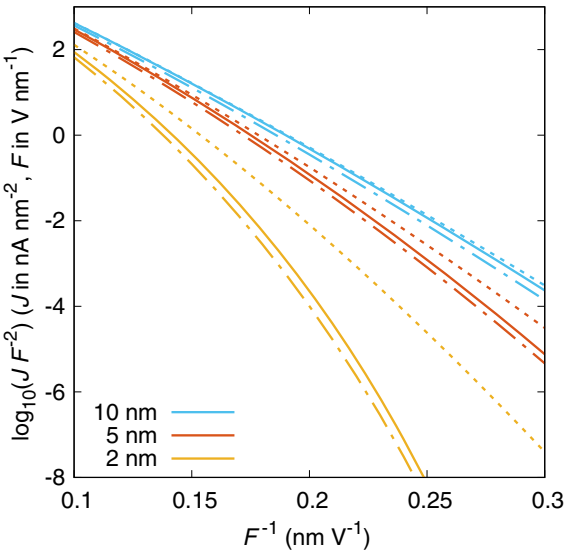

FIG. 5. Fowler-Nordheim plot for the zero-temperature FN-type equation, Eq. (33), evaluated using $v^*(t, A)$ and $t^*(y, A)$ from Kyritsakis and Xanthakis's formulas [Eqs. (19) and (21), dashed lines] and a least-squares fit to the numerical data [Eqs. (A2) and (A7), dotted-dashed lines]. The precise numerical calculation of Eq. (5) at 300 K is given by the solid lines.

$$J_T(F, T) = \lambda(T) J_0(F), \tag{31}$$

where $J_0(F)$ is the zero-temperature emitted current density and $\lambda(T)$ is a temperature correction factor given by

$$\lambda(T) = \frac{\pi c k_B T}{\sin(\pi c k_B T)}. \tag{32}$$

Clearly, $\lambda(T)$ tends to unity as T goes to zero.

The zero-temperature emitted current density $J_0(F)$ is given by

$$J_0(F) = \frac{a_{\mathrm{FN}}}{t^{*2}(y_0, A)} \frac{F^2}{\phi} \exp\left[-b_{\mathrm{FN}} \frac{\phi^{3/2}}{F} v^*(y_0, A)\right], \tag{33}$$

where a_{FN} and b_{FN} are universal constants called the first and second FN constants [5]; the value of b_{FN} is provided by Eq. (15), while

$$a_{\mathrm{FN}} = z_s \left(\frac{2}{3 b_{\mathrm{FN}}}\right)^2 \approx 1.541\,434\ \mu\mathrm{A\,eV\,V^{-2}}. \tag{34}$$

The only differences between the planar and spherical situations lie in the mathematical form of the correction factors $v^*(y, A)$ and $t^*(y, A)$ and in the different values of $v^*(y_0, A)$, $t^*(y_0, A)$, and c. This functional dependence indicates that Eqs. (31) and (33) are in the form of core FN-type equations [36], which, in this instance, describe cold-field emission from an earthed spherical emitter. In this paper, Eqs. (31) and (33) are simply referred to as the finite- and zero-temperature FN-type equations, respectively.

The zero-temperature FN-type equation, Eq. (33), is compared to the exact current density, as calculated from Eq. (5), in Fig. 4 for various planar and spherical emitters, with $\phi = 4.5$ eV at $T = 300$ K. At this temperature, Eqs. (33) and (31) are indistinguishable. This plot utilizes the approximate formulas for $v^*(y, A)$ and $t^*(y, A)$, which are provided by Eqs. (A2) and (A7) in the Appendix. For very strong electric fields, the field-induced regime approximations are invalid, as the lower limit of the integral in Eq. (29) cannot be arbitrarily taken to be $-\infty$, and doing so produces an overestimation of the emitted current density.

The base-10 logarithm of the current density calculated from the zero-temperature FN-type equation is plotted as a function of $1/F$ in Fig. 5; such a plot is commonly referred to as a Fowler-Nordheim plot and is useful for characterizing cold-field electron emitters. Equation (33) is plotted using the exact barrier-form correction factors, as given by a direct numerical evaluation of Eqs. (16) and (20), the approximate formulas provided by Kyritsakis and Xanthakis [20], Eqs. (19) and (21), and the least-squares fits provided in the Appendix, Eqs. (A2) and (A7), for spherical emitters with radii 10, 5, and 2 nm. This plot exhibits a changing slope which is typical of nontriangular surface potential barriers [37]. The results support Kyritsakis and Xanthakis's conclusion that their formulas are satisfactory for emitters of radius 5 nm $< a <$ 10 nm. The formulas provided in the Appendix provide improved approximations for the barrier-form correction functions for emitters smaller than 5 nm.

The FN-type equations can fail at any given value of F for sufficiently high temperatures, as the JWKB approximation,

Eq. (22), and the linear expansion of $G(W,F)$, Eq. (23), may no longer be applied. The details of these issues are discussed in Sec. VI, below which defines, in F-T parameter space, an upper boundary for the cold-field-emission region, and hence the limits of validity for the FN-type equations. Within this boundary, the FN-type equations provide a good concise working formula for estimating emission current density.

V. THERMAL EMISSION

Equation (5) may also be evaluated analytically in the high-temperature, low-field regime, which is often referred to as the barrier-top-emission regime. In this case, the emitted current is dominated by electrons with energies around the barrier peak, where $(W-E_F)\gg k_BT$ even at high temperatures, allowing the approximation

$$\ln\left[1+\exp\left(-\frac{W-E_F}{k_BT}\right)\right]\simeq\exp\left(-\frac{W-E_F}{k_BT}\right) \tag{35}$$

to be made. The expansion of $G(W,F)$ is now performed around the peak of the barrier. If the peak height of the spherical barrier in Fig. 1, as measured from the base of the conduction band, is denoted as H_m and the corresponding value of y as $y_m=c_sF^{1/2}/H_m$, then an appropriate small parameter is

$$\epsilon=1-\frac{H}{H_m}=\frac{y_m}{c_sF^{1/2}}\left(\frac{c_sF^{1/2}}{y_m}+W-E_F-\phi\right). \tag{36}$$

This parameter is useful as it is both linear in W and zero at the barrier peak. It is also used in Sec. VI A to evaluate the limits of the field-emission regime. $G(W,F)$ vanishes at the barrier peak since Eq. (17) has a repeated root, $\rho_1=\rho_2$, and hence $v^*(y_m,A)=0$. The expansion follows from Eq. (14) as

$$\begin{aligned}G(W,F)&=b_{\mathrm{FN}}\frac{c_s^{3/2}}{F^{1/4}}y^{-3/2}v^*(y,A)\\&\approx b_{\mathrm{FN}}\frac{c_s^{3/2}}{F^{1/4}}\left(-\frac{3}{2}\frac{t^*(y_m,A)}{y_m^{3/2}}\epsilon+\frac{3}{8}\frac{u^*(y_m,A)}{y_m^{3/2}}\epsilon^2\right)\\&\approx\frac{-1}{k_BTq}\left(\frac{c_sF^{1/2}}{y_m}+W-E_F-\phi\right),\end{aligned} \tag{37}$$

where only the first term is retained in the last line and

$$q^{-1}=-\frac{3k_BTb_{\mathrm{FN}}c_s^{1/2}}{2F^{3/4}}\frac{t^*(y_m,A)}{y_m^{1/2}}. \tag{38}$$

This expansion reproduces those given by Murphy and Good [9] and Modinos [1] in the planar limit for which $y_m=1$ and $t^*(y_m,A\to\infty)=\pi/\sqrt{8}$. Note, again, that the series expansion is simplified by the independence of A from W.

With the approximations of Eqs. (35) and (37) made, Eq. (5) becomes

$$\begin{aligned}&J(F,T)\\&=z_sk_BT\\&\quad\times\int_0^\infty\frac{\exp[-(W-E_F)/k_BT]dW}{1+\exp[-(c_sF^{1/2}/y_m+W-E_F-\phi)/k_BTq]}.\end{aligned} \tag{39}$$

The integrand drops off quickly as W moves downwards from the level of the top of the barrier, so the lower limit can be replaced by $-\infty$, and making the substitution

$$\mu=\exp\left[\frac{-1}{k_BTq}\left(\frac{c_sF^{1/2}}{y_m}+W-E_F-\phi\right)\right] \tag{40}$$

yields

$$\begin{aligned}J(F,T)&=z_sq(k_BT)^2\int_0^\infty\frac{\mu^{q-1}}{1+\mu}d\mu\\&\quad\times\exp\left[\frac{-1}{k_BT}\left(\phi-\frac{c_sF^{1/2}}{y_m}\right)\right].\end{aligned} \tag{41}$$

This is the same standard form as in Eq. (30) and, provided that $q<1$, the integral converges to give the extended RS-type equation [35]

$$J(F,T)=z_s(k_BT)^2\frac{\pi q}{\sin(\pi q)}\exp\left[\frac{-1}{k_BT}\left(\phi-\frac{c_sF^{1/2}}{y_m}\right)\right]. \tag{42}$$

In the limit of weak applied fields, when $\pi q\ll 1$, this reduces to the RS-type equation

$$J(F,T)=A_RT^2\exp\left[\frac{-1}{k_BT}\left(\phi-\frac{c_sF^{1/2}}{y_m}\right)\right], \tag{43}$$

where Richardson's constant is

$$A_R=z_sk_B^2=1.201735\times10^6\ \mathrm{A\,m^{-2}\,K^{-2}}. \tag{44}$$

As with the field-emission regime, the only difference between the spherical and planar cases is from the differing values of y_m and $t^*(y_m,A)$, for which approximate formulas are provided in the Appendix. A plot of the logarithm of the emitted current density, according to Eq. (43), against $F^{1/2}$ gives a straight line of slope c_s/y_m; such a plot is known as a Schottky plot [1], and the slope is reduced for small spheres.

The current densities given by Eq. (43)—calculated using Eq. (A9) for y_m, as provided in the Appendix—are displayed in Fig. 6 and are compared with the precise numerical evaluation of Eq. (5). Within the thermal-emission

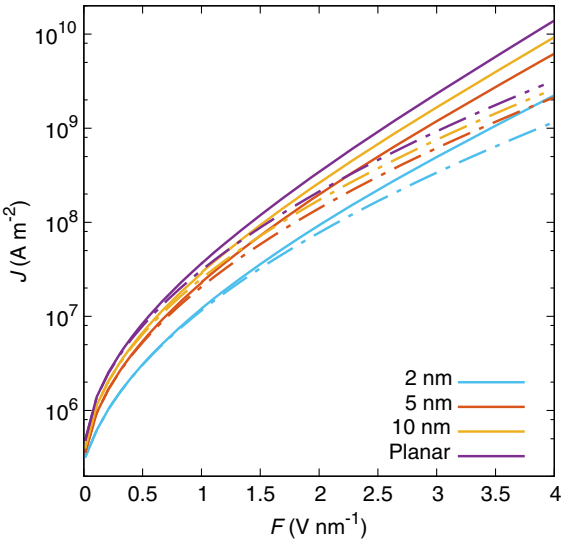

FIG. 6. Thermal current densities from surfaces with $\phi = 4.5$ eV and $T = 3000$ K, as calculated using the RS-type equation, Eq. (43), with y_m provided by Eq. (A9) (dotted-dashed lines), and the precise numerical solution of Eq. (5) (solid lines).

region, the boundaries of which are considered in Sec. VI, the RS-type equation reproduces the numerical solutions. The spherical current densities tend to the planar values for large spheres, and the spherical and planar current densities are identical for $F = 0$, as the potential barrier is essentially removed in this case. The effect of sphericity is, in general, to significantly reduce the emitted current at any given value of F. This reduction is due to the spherical potential barrier increasing in height for decreasing values of A, as demonstrated in Fig. 1, so that y_m increases and the emitted current falls.

VI. VALIDITY OF APPROXIMATIONS

A number of approximations have been made in the preceding subsections and, while the resulting FN-type and extended RS-type equations [Eqs. (31) and (42), respectively] are of great utility, the validity of these approximations must be carefully considered. This consideration is made here following the methodology of Murphy and Good [9]. An alternative test was performed by Bahm *et al.* [38], who calculated the transmission coefficient using an exact solution of the Schrödinger equation, rather than the JWKB-type approximation, and found the results deviate from the planar FN-type equation for $ck_BT > 0.7$ and from the extended RS-type equation for $q > 0.25$. Such a test of the spherical equations is, however, a significant work in itself and is beyond the immediate scope of this paper.

A. Field-induced emission

The derivation of the field-induced emitted current requires that the conditions

$$G(W, F) > 1 \tag{45}$$

and

$$|f|(W - E_F)^2 < \frac{1}{2} \tag{46}$$

are satisfied in order to neglect higher-order terms in the expansions of Eqs. (22) and (23). Equation (45) is violated for electron energies close to the barrier peak; the expansion in terms of $G(W, F)$ in terms of ϵ, Eq. (37), is therefore suitable and allows Eq. (45) to be rewritten as

$$W - E_F < \phi - k_BTq - \frac{c_sF^{1/2}}{y_m}. \tag{47}$$

The conditions in Eqs. (46) and (47) must be valid for electrons which make a significant contribution to the emitted current. Murphy and Good identify these significant contributions as those from electrons with energies for which the integrand of Eq. (29) is greater than $\exp(-1)$ of its maximum value. This defines an upper limit for the energy of such electrons as

$$W - E_F < \frac{k_BT}{1 - ck_BT}. \tag{48}$$

Inequalities which define the field-induced emission region are found through a comparison of Eqs. (46) and (47) to Eq. (48). These inequalities are

$$\phi - \frac{k_BT}{1 - ck_BT} > \frac{c_sF^{1/2}}{y_m} + k_BTq \tag{49}$$

and

$$1 - ck_BT > (2f)^{1/2}k_BT. \tag{50}$$

The field-emission region given by these inequalities is shaded blue in Fig. 7 for various spherical and planar surfaces with $\phi = 4.5$ eV. Field emission cannot occur when $\phi < eFa$, as this implies that the potential barrier never falls below the Fermi energy even at large distances from the sphere, which is particularly evident at $F = 2.25$ V nm^{-1} for $a = 2$ nm. Electrons are, generally, quite unlikely to tunnel through the broad potential barriers of small spherical surfaces; this effect causes a significant reduction in the size of the field-emission region for very small spherical emitters.

B. Thermal emission

The thermal-emission region must also be defined. The expansion in Eq. (35) may be truncated at first order when

$$W - E_F > k_BT \tag{51}$$

is satisfied, while neglecting the quadratic term in ϵ in Eq. (37) is justified when

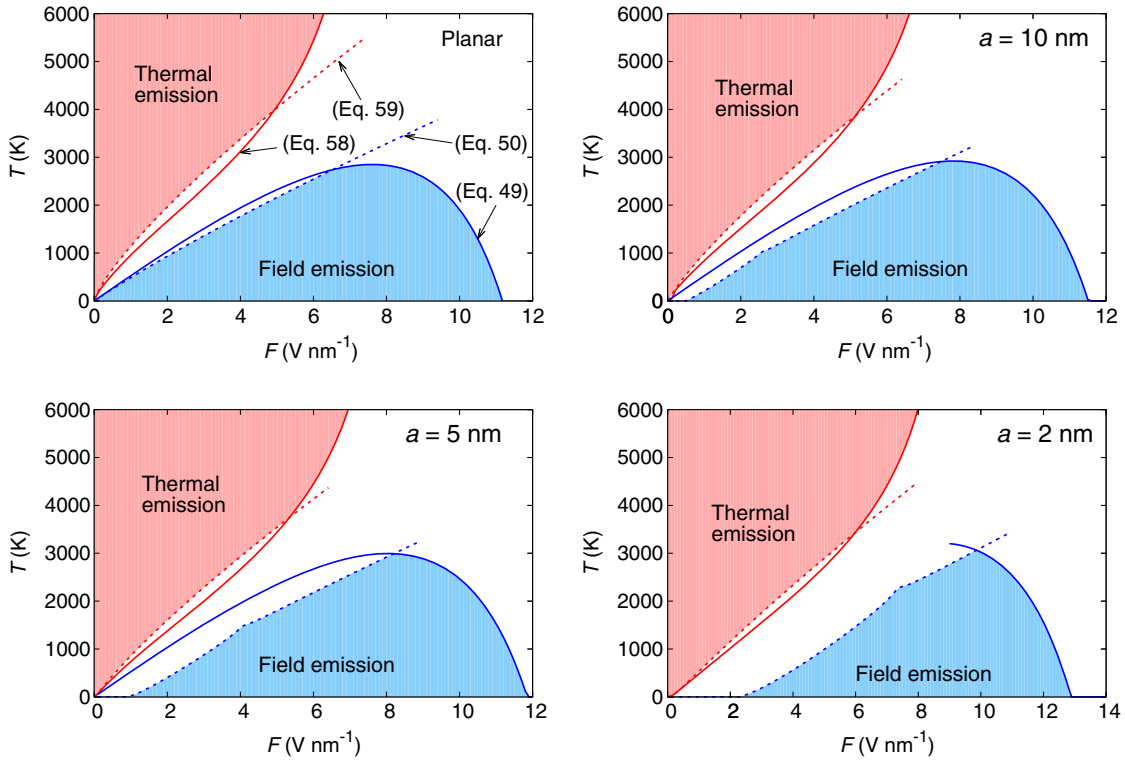

FIG. 7. The field-emission region, as defined by Eqs. (49) (blue, solid line) and (50) (blue, dashed line), and the thermal-emission region, according to Eqs. (58) (red, solid line) and (59) (red, dashed line), for various emitters with $\phi = 4.5$ eV.

$$\epsilon > -\frac{F^{1/8}}{b_{\mathrm{FN}}^{1/2} c_s^{3/4}}, \tag{52}$$

which, using the definition of ϵ in Eq. (36), is equivalent to

$$W - E_F > \phi - \frac{c_s^{1/4} F^{5/8}}{y_m b_{\mathrm{FN}}^{1/2}} - \frac{y_m}{c_s F^{1/2}}. \tag{53}$$

These conditions must again be satisfied for electron energies which make a significant contribution to the emitted current. The integrand I in Eq. (39) has a maximum when $(W - E_F)$ takes the value

$$\eta = \phi - \frac{c_s F^{1/2}}{y_m} - k_B T q \ln\left(\frac{q}{1-q}\right) \tag{54}$$

and decreases roughly like

$$I \propto \exp\left(-\frac{W - E_F}{k_B T}\right) \tag{55}$$

for values of $(W - E_F) > \eta$, and roughly like

$$I \propto \exp\left(-\frac{W - E_F}{k_B T}\right) \exp\left(\frac{W - E_F}{k_B T q}\right) \tag{56}$$

for values of $(W - E_F) < \eta$. The integrand is therefore larger than $\exp(-1)$ of its maximum value over the range

$$k_B T > (W - E_F) - \eta > -\frac{k_B T q}{1-q}, \tag{57}$$

which corresponds to the range of significant contributions to the current for which the conditions in Eqs. (51) and (53) must hold. The thermal-emission region condition is, therefore, defined by the inequalities

$$\ln\left(\frac{1-q}{q}\right) - \frac{1}{q(1-q)} > \frac{1}{k_B T q}\left(\frac{c_s F^{1/2}}{y_m} - \phi\right), \tag{58}$$

as found by comparing Eq. (51) to the lower limit of Eq. (57), and

$$\ln\left(\frac{1-q}{q}\right) - \frac{1}{1-q} > -\frac{1}{k_B T q}\frac{c_s^{1/4} F^{5/8}}{y_m b_{\mathrm{FN}}^{1/2}}, \tag{59}$$

as found by comparing Eq. (53) to the lower limit of Eq. (57). The regions defined by these limits are illustrated by the red shaded regions in Fig. 7. Unlike the field-emission region, the thermal region increases in size for spherical surfaces with smaller radii. This effect arises from the broadening of the spherical potential barrier which suppresses tunneling and gives currents which are dominated by thermally excited electrons near the barrier peak.

VII. SPECTRA OF EMITTED ELECTRONS

It can be useful to know the distribution of energies of the emitted electrons, in addition to the total emitted current. The number of emitted electrons with total energy between E and $E + dE$, per energy increment dE, is given by the free-electron theory as

$$j(E, F, T) = z_s f_{\mathrm{FD}}(E, T) \int_0^E D(W, F) dW. \quad (60)$$

The expression for the total current density, Eq. (5), can be retrieved by integrating $j(E, F, T)$ over all electron energies,

$$J(F, T) = \int_0^\infty j(E, F, T) dE, \quad (61)$$

and making the substitution $E = W + E_p$. Equation (60) may be evaluated exactly using the expressions for $f_{\mathrm{FD}}(E, T)$ and $D(W, F)$, from Eqs. (3) and (7), or evaluated approximately in the thermal or field-induced regimes.

The energy spectra of thermally emitted electrons may be crudely approximated by taking the transmission coefficient, $D(W)$, as 1 when W is larger than the potential energy of the barrier peak, denoted as V_m, and 0 when it is below the peak. The Fermi-Dirac function becomes proportional to $\exp(-E/k_B T)$ in the thermal regime, and the integral in Eq. (60) can be immediately evaluated to give

$$j_T(E) \propto (E - V_m) \exp\left[\frac{-(E - E_F)}{k_B T}\right]. \quad (62)$$

This distribution is compared to the precise numerical solution of Eq. (60) in Fig. 8 for spheres with $\phi = 4.5$ eV and of radius 2 or 10 nm. Equation (62) is shown to be a good approximation of the numerical results, although the low-energy tail of electrons which tunnel through the barrier is truncated. The values of $E_F + \phi - V_m$, as found from the values of y_m given in the Appendix, are 1.147 and 2.347 eV for the 10-nm sphere with $F = 1$ V nm^{-1} and $F = 4$ V nm^{-1}, respectively, and 0.945 and 2.138 eV for the 2-nm sphere with $F = 1$ V nm^{-1} and $F = 4$ V nm^{-1}.

The field-induced energy distribution, first derived for the planar case by Young [39], follows from the approximations of Eqs. (22) and (23). Performing the integral in Eq. (60) yields

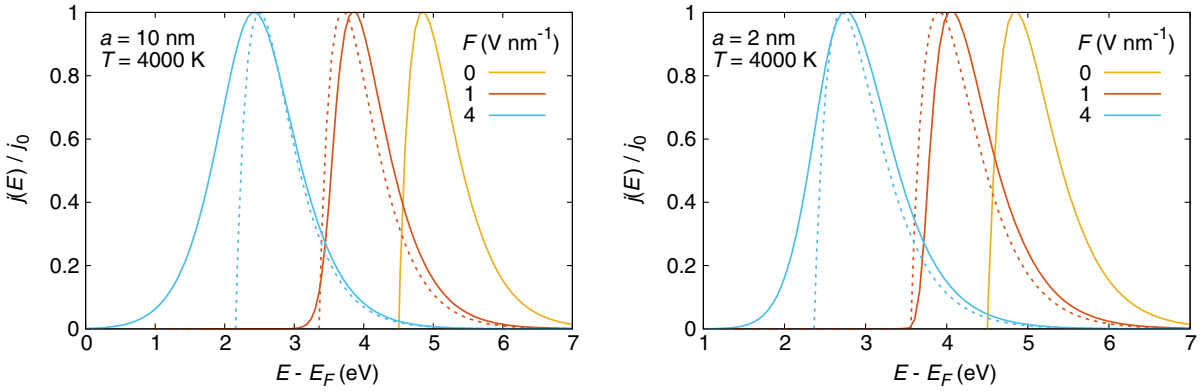

FIG. 8. The energy distributions of thermally emitted electrons from surfaces with $\phi = 4.5$ eV. Numerical solutions, calculated from Eq. (60), are plotted as solid lines, while approximate solutions, from Eq. (62), are given by the broken lines.

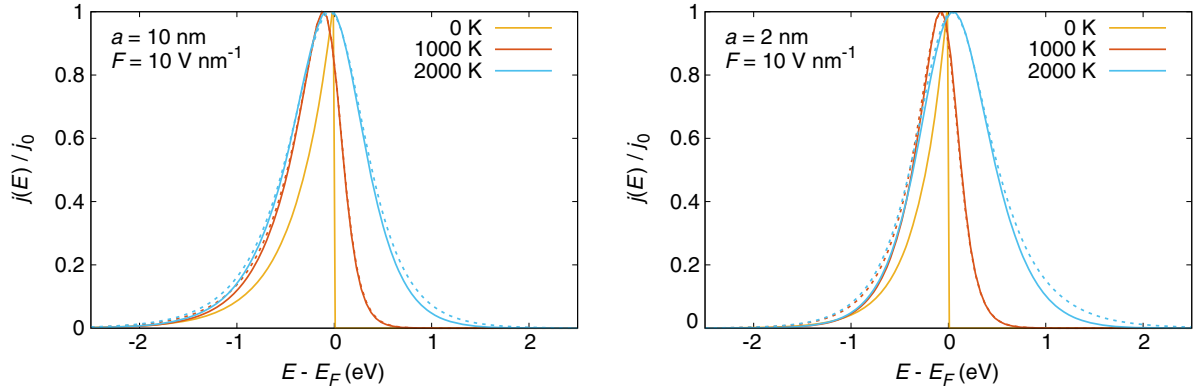

FIG. 9. The energy distributions of field-emitted electrons for the same-sized spheres as Fig. 8. Approximate spectra, given by Eq. (63), are plotted as dashed lines, while the precise numerical solutions of Eq. (60) are shown by solid lines.

$$j_F(E) = \frac{z_s}{c}\frac{\exp[-b + c(E - E_F)]}{1 + \exp[(E - E_F)/k_B T]}, \qquad (63)$$

where b and c are given by Eqs. (24) and (25). The finite-temperature FN-type equation, as given by Eq. (31), may be derived by integrating $j_F(E)$ over all values of E, as suggested by Eq. (61). Equation (63) is compared to the precise numerical solution of Eq. (60) in Fig. 9. The approximate spectra give excellent estimates of the emitted electron energy distributions in the cases shown.

VIII. SUMMARY

The standard formulas for the emission of electrons from planar surfaces are unsuitable for highly curved surfaces and can lead to significant order-of-magnitude errors when incorrectly applied. In this paper, accurate equations for the emission current densities from earthed nanoscale spherical surfaces are derived. These expressions are applicable to metallic electron emitters in many modern applications, which can be only a few nanometers in size.

The theory of electron emission from earthed spherical surfaces is developed using the framework of Murphy and Good's unified emission theory. This provides a route to the spherical FN-type equation for field-induced emission, Eq. (31), and the spherical RS-type equation for thermal emission, Eq. (43). The tables and approximate fits for the barrier-form correction functions $v^*(y, A)$ and $t^*(y, A)$, which are provided in the Appendix, allow straightforward evaluation of these two equations for a wide range of values of radius, field strength, temperature, and material work function. These functions also provide an extension to the series solutions found by Kyritsakis and Xanthakis [20], which produce the same results in the expected limit $yA \gg 1$. The spherical FN- and RS-type equations are shown to match the precise numerically evaluated currents, calculated directly from Eq. (5), for tungsten-relevant parameters over certain ranges of validity; Sec. VI carefully considers these ranges of validity and shows that emission from small earthed spheres is more often dominated by thermal effects than field effects. Finally, the energy spectra of thermally emitted and field-emitted electrons from earthed spherical surfaces are calculated in Sec. VII and the approximate spectra are compared with the precise numerically evaluated values for some tungsten-relevant examples.

The differences between the planar and spherical emission theories arise primarily because the potential barrier at the surface of a spherical emitter is taller and wider than that of a planar emitter for the same strength of applied electric field, which leads to much smaller emitted currents when comparing emitters with the same surface field strengths. However, when comparing electrodes with the same surface voltage, spherical anodes will produce a larger surface electric field and hence can produce much larger emitted currents than planar surfaces. This behavior corroborates previous findings that the enhanced field-induced emission from needlelike anodes is principally due to the enhancement of electric field at highly curved, nanometer-scale surfaces [19,40].

The approach taken here could be extended to other situations where the electric potential at the emitter surface is described by an arbitrary 1D function. Any parameters which are introduced to describe the shapes of different potential barriers, such as A in this paper, must be kept independent of the normal electron energy, W, so that the series expansions required by the Murphy and Good methodology remain independent of these new parameters. Possible examples include isolated spheres, which are of interest in areas such as volcanic-ash plumes [41] and small objects in plasmas [42], space-charge-regime emission, where the emitted electrons contribute significantly to the electric potential [43,44], and emission from planar electrodes in contact with plasmas where the Bohm sheath provides a simple model for the potential barrier [45].

ACKNOWLEDGMENTS

This work was supported by an Imperial College President's Ph.D. Scholarship and an Aerosol Society C. N. Davies Award. Extremely useful comments from the referees are gratefully acknowledged.

APPENDIX: REFERENCE TABLES AND APPROXIMATE FORMULAS FOR THE BARRIER-FORM CORRECTION FUNCTIONS

The calculations of the field-induced and thermal currents and their ranges of validity require the barrier-form correction functions $v^*(y, A)$, $t^*(y, A)$, and $u^*(y, A)$ to be evaluated. These fits are used to produce the figures and examples given in the main part of this paper.

The values of A to be considered are determined by the parameter ranges of $F < 15\,\mathrm{V\,nm^{-1}}$ and $2\,\mathrm{nm} < a < 100\,\mathrm{nm}$, which, using the definition of A in Eq. (13), corresponds to $A \geq 1$.

In Sec. VI A, it is found that field emission cannot occur when $\phi > eFa$, which is equivalent to requiring $yA > 1$ for emission to occur. When this condition is not satisfied, there is only one root of Eq. (17) and the barrier-form correction functions cannot be evaluated. Furthermore, the values of y which are greater than y_m, corresponding to normal electron energies higher than the barrier peak, are not relevant for calculating field-induced or thermal currents and are also omitted from the tabulated values provided here.

The exact values of y_m, $v^*(y, A)$, $t^*(y, A)$, $t^*(y_m, A)$, and $u^*(y, A)$ are given in Tables I, II, and III. The values of $v^*(y, A)$ and $t^*(y, A)$ corresponding to emission from a planar surface are given by $A = \infty$ and are provided by the tables of Burgess *et al.* [8]. As expected, the spherical functions tend to the planar values in the large-A limit.

The best fit for the planar function is taken as a starting point for finding a suitable approximation for $v^*(y, A)$. Forbes [33] provides the formula

TABLE I. Exact and approximate values of $v^*(y,A)$, from Eqs. (16) and (A2), respectively, with the latter shown in parentheses next to the corresponding exact values. The values of y_m and the approximate fit of Eq. (A9), again given in parentheses, are provided in the bottom row.

		A							
		1	2	5	10	20	50	100	∞
y	0	⋯	⋯	⋯	⋯	⋯	⋯	⋯	1.0000
	0.1	⋯	⋯	⋯	⋯	1.693 (1.895)	1.175 (1.288)	1.069 (1.152)	0.9817
	0.2	⋯	⋯	⋯	1.645 (1.696)	1.190 (1.247)	1.024 (1.073)	0.979 (1.017)	0.9370
	0.3	⋯	⋯	2.167 (2.169)	1.241 (1.266)	1.025 (1.059)	0.927 (0.959)	0.899 (0.924)	0.8718
	0.4	⋯	⋯	1.483 (1.497)	1.036 (1.058)	0.897 (0.923)	0.829 (0.853)	0.809 (0.828)	0.7888
	0.5	⋯	⋯	1.160 (1.190)	0.874 (0.894)	0.773 (0.794)	0.721 (0.740)	0.705 (0.721)	0.6900
	0.6	⋯	3.255 (3.398)	0.928 (0.963)	0.721 (0.740)	0.643 (0.661)	0.602 (0.618)	0.589 (0.602)	0.5768
	0.7	⋯	1.946 (2.117)	0.726 (0.764)	0.568 (0.586)	0.505 (0.521)	0.471 (0.485)	0.461 (0.471)	0.4504
	0.8	⋯	1.339 (1.529)	0.536 (0.573)	0.409 (0.427)	0.357 (0.372)	0.329 (0.341)	0.320 (0.330)	0.3117
	0.9	⋯	0.931 (1.114)	0.347 (0.385)	0.243 (0.263)	0.200 (0.215)	0.176 (0.188)	0.169 (0.177)	0.1613
	1.0	⋯	0.604 (0.769)	0.155 (0.197)	0.069 (0.093)	0.033 (0.050)	0.013 (0.025)	0.006 (0.015)	0.0000
	1.1	4.156 (4.230)	0.316 (0.462)	⋯	⋯	⋯	⋯	⋯	⋯
	1.2	2.107 (2.093)	0.046 (0.182)	⋯	⋯	⋯	⋯	⋯	⋯
	1.3	1.146 (1.107)	⋯	⋯	⋯	⋯	⋯	⋯	⋯
	1.4	0.510 (0.443)	⋯	⋯	⋯	⋯	⋯	⋯	⋯
	1.5	0.014 (−0.059)	⋯	⋯	⋯	⋯	⋯	⋯	⋯
y_m		1.503 (1.503)	1.218 (1.218)	1.080 (1.079)	1.039 (1.038)	1.019 (1.019)	1.0075 (1.0074)	1.0038 (1.0037)	1.0000

TABLE II. Exact values of the functions $t^*(y,A)$ and $t^*(y_m,A)$, calculated directly from Eq. (20), compared to the approximate fits of Eqs. (A7) and (A10), respectively; the values from the approximate fits are given in parentheses.

		A							
		1	2	5	10	20	50	100	∞
y	0	⋯	⋯	⋯	⋯	⋯	⋯	⋯	1.0000
	0.1	⋯	⋯	⋯	⋯	2.572 (3.124)	1.353 (1.565)	1.155 (1.300)	1.0036
	0.2	⋯	⋯	⋯	2.579 (2.733)	1.483 (1.590)	1.162 (1.248)	1.082 (1.148)	1.0111
	0.3	⋯	⋯	4.551 (4.634)	1.747 (1.785)	1.297 (1.356)	1.117 (1.171)	1.067 (1.109)	1.0207
	0.4	⋯	⋯	2.594 (2.551)	1.501 (1.529)	1.226 (1.269)	1.102 (1.142)	1.066 (1.098)	1.0319
	0.5	⋯	⋯	2.032 (2.028)	1.389 (1.415)	1.194 (1.228)	1.099 (1.131)	1.071 (1.097)	1.0439
	0.6	⋯	12.259 (12.703)	1.775 (1.798)	1.329 (1.353)	1.178 (1.206)	1.102 (1.128)	1.079 (1.100)	1.0565
	0.7	⋯	5.669 (5.663)	1.631 (1.667)	1.294 (1.314)	1.171 (1.194)	1.108 (1.130)	1.089 (1.107)	1.0697
	0.8	⋯	3.876 (4.051)	1.543 (1.579)	1.273 (1.287)	1.171 (1.187)	1.117 (1.134)	1.010 (1.114)	1.0832
	0.9	⋯	3.073 (3.345)	1.484 (1.511)	1.261 (1.266)	1.173 (1.182)	1.126 (1.138)	1.111 (1.122)	1.0969
	1.0	⋯	2.627 (2.920)	1.444 (1.454)	1.255 (1.247)	1.178 (1.178)	1.137 (1.143)	1.124 (1.130)	1.1107
	1.1	29.623 (32.249)	2.346 (2.607)	⋯	⋯	⋯	⋯	⋯	⋯
	1.2	12.219 (12.373)	2.156 (2.340)	⋯	⋯	⋯	⋯	⋯	⋯
	1.3	7.642 (7.866)	⋯	⋯	⋯	⋯	⋯	⋯	⋯
	1.4	5.637 (5.761)	⋯	⋯	⋯	⋯	⋯	⋯	⋯
	1.5	4.537 (4.354)	⋯	⋯	⋯	⋯	⋯	⋯	⋯
$t^*(y_m,A)$		4.510 (4.510)	2.129 (2.129)	1.421 (1.420)	1.254 (1.255)	1.179 (1.180)	1.138 (1.138)	1.124 (1.124)	1.1107

$$v(y) = 1 - y^2 + \frac{y^2\ln(y)}{3}, \tag{A1}$$

which gives $v(y)$ within 0.33% of its exact value for $0 \le y \le 1$. From Fig. 2 and the values in Table I, it is noted that $v^*(y,A)$ tends to infinity as $y \to 1/A$; this suggests that a suitable functional form could be

$$v^*(y,A) = \alpha(A) - \beta(A)y^2 + \delta(A)\frac{y^2\ln(y)}{3} + \frac{\varepsilon(A)}{y - 1/A}, \tag{A2}$$

where α, β, δ, and ε are determined by a least-squares fitting of $v^*(y,A)$ to its exact values as

$$\alpha(A) = 1 + \frac{4.9}{A^2}, \tag{A3}$$

$$\beta(A) = 1 + \frac{3.5}{A^2}, \tag{A4}$$

$$\delta(A) = 0.334 + \frac{0.6}{A} + \frac{2.9}{A^2}, \tag{A5}$$

TABLE III. Exact values of the function $u^*(y,A)$, from Eq. (28), alongside the approximate fits according to Eq. (A8). The fit fails to provide good estimates of $u^*(y,A)$ and is particularly poor for small values of A.

		A						
		1	2	5	10	20	50	100
y	0	⋯	⋯	⋯	⋯	⋯	⋯	⋯
	0.1	⋯	⋯	⋯	⋯	11.080 (13.969)	3.451 (3.088)	2.166 (1.981)
	0.2	⋯	⋯	⋯	7.805 (11.316)	3.034 (3.252)	1.656 (1.761)	1.284 (1.408)
	0.3	⋯	⋯	13.760 (34.225)	3.357 (4.240)	1.855 (2.133)	1.254 (1.436)	1.081 (1.232)
	0.4	⋯	⋯	5.360 (9.340)	2.174 (2.799)	1.433 (1.729)	1.107 (1.283)	1.011 (1.138)
	0.5	⋯	⋯	3.204 (5.229)	1.667 (2.223)	1.240 (1.521)	1.045 (1.191)	0.988 (1.078)
	0.6	⋯	31.221 (223.089)	2.283 (3.791)	1.407 (1.927)	1.144 (1.398)	1.022 (1.130)	0.986 (1.036)
	0.7	⋯	10.816 (43.090)	1.798 (3.126)	1.264 (1.759)	1.097 (1.321)	1.019 (1.090)	0.996 (1.008)
	0.8	⋯	5.810 (19.611)	1.517 (2.745)	1.184 (1.663)	1.078 (1.275)	1.028 (1.065)	1.013 (0.990)
	0.9	⋯	3.715 (12.711)	1.347 (2.614)	1.142 (1.614)	1.076 (1.251)	1.044 (1.054)	1.034 (0.983)
	1.0	⋯	2.608 (9.993)	1.244 (2.549)	1.123 (1.602)	1.084 (1.248)	1.064 (1.054)	1.059 (0.986)
	1.1	57.641 (1141.05)	1.944 (8.840)	⋯	⋯	⋯	⋯	⋯
	1.2	17.989 (190.149)	1.517 (8.847)	⋯	⋯	⋯	⋯	⋯
	1.3	8.487 (80.443)	⋯	⋯	⋯	⋯	⋯	⋯
	1.4	4.492 (51.593)	⋯	⋯	⋯	⋯	⋯	⋯
	1.5	2.187 (41.612)	⋯	⋯	⋯	⋯	⋯	⋯

$$\varepsilon(A) = \frac{1}{3A^{2/3}}. \tag{A6}$$

The approximate values of $v^*(y,A)$ provided by this fit are given in Table I in parentheses alongside the corresponding exact values. These values show that the fit is reasonably good except for values of y approaching y_m; these are not relevant for field-induced emission, where $W \simeq E_F$, but a better fit in the vicinity of y_m is required for an accurate calculation of the thermal currents.

The function $t^*(y,A)$, defined by Eq. (20), follows as

$$t^*(y,A) = \alpha + \left(\frac{\beta}{3} - \frac{2\delta}{3}\right)y^2 - \frac{\delta}{3}y^2\ln(y) + \frac{\varepsilon}{y-1/A} + \frac{2\varepsilon y}{3(y-1/A)^2}, \tag{A7}$$

and its approximate values, as provided by the least-squares fit, are given in parentheses alongside the exact values in Table II. The field-emission results shown as dashed curves in Figs. 4 and 5 are calculated from the FN-type equation, Eq. (31), with barrier-form correction functions given by these fits for $v^*(y,A)$ and $t^*(y,A)$.

The function $u^*(y,A)$, which is given by Eq. (28) and is required for evaluating the limit of validity of the field-induced approximation in Eq. (50), is also determined from

$$u^*(y,A) = \alpha + \left(\frac{8\delta}{3} - \beta\right)y^2 - \delta y^2\ln(y) + \frac{\varepsilon}{y-1/A} + \frac{4\varepsilon y}{3(y-1/A)^2} + \frac{8\varepsilon y^2}{3(y-1/A)^3}. \tag{A8}$$

Again, the values given by the least-squares fit are given in parentheses next to the corresponding exact values in Table III. These values are a relatively poor fit to the exact values and an exact calculation of $u^*(y,A)$ is recommended for determining the field-induced emission limits. The field-emission regions in Fig. 7 are produced using the exact values for $u^*(y,A)$ rather than the fitted values.

The approximate formulas provided so far become inaccurate for electron energies close to the potential barrier peak. It is more convenient to consider separate least-squares fits for y_m and $t^*(y_m,A)$, such as

$$y_m = 1 + \frac{0.369}{A} + \frac{0.134}{A^2}, \tag{A9}$$

$$t^*(y_m,A) = 1.1107 + \frac{1.357}{A} + \frac{0.676}{A^2} + \frac{1.366}{A^3}. \tag{A10}$$

These formulas are used along with the Schottky equation, Eq. (43), to produce the dashed curves for thermal emission in Fig. 6 and provide excellent fits to the exact values, as shown by the parenthetical values in the last rows of Tables I and II.

[1] A. Modinos, *Field, Thermionic, and Secondary Electron Emission Spectroscopy* (Plenum, New York, 1984).

[2] O. W. Richardson, *The Emission of Electricity from Hot Bodies* (Longmans, Green, London, 1921).

[3] R. H. Fowler, The restored electron theory of metals and thermionic formulae, Proc. R. Soc. A **117**, 549 (1928).

[4] W. Schottky, Cold and hot electron discharges, Z. Phys. **14**, 63 (1923).

[5] R. G. Forbes and J. H. B. Deane, Transmission coefficients for the exact triangular barrier: An exact general analytical theory that can replace Fowler & Nordheim's 1928 theory, Proc. R. Soc. A **467**, 2927 (2011).
[6] L. W. Nordheim, The effect of the image force on the emission and reflexion of electrons by metals, Proc. R. Soc. A **121**, 626 (1928).
[7] R. H. Fowler and L. W. Nordheim, Electron emission in intense electric fields, Proc. R. Soc. A **119**, 173 (1928).
[8] R. E. Burgess, H. Kroemer, and J. M. Houston, Corrected values of Fowler-Nordheim field emission functions $v(y)$ and $s(y)$, Phys. Rev. **90**, 515 (1953).
[9] E. L. Murphy and R. H. Good, Jr., Thermionic emission, field emission, and the transition region, Phys. Rev. **102**, 1464 (1956).
[10] S. G. Christov, Recent test and new applications of the unified theory of electron emission, Surf. Sci. **70**, 32 (1978).
[11] K. L. Jensen, General formulation of thermal, field, and photoinduced electron emission, J. Appl. Phys. **102**, 024911 (2007).
[12] J. He, P. H. Cutler, and N. M. Miskovsky, Generalization of Fowler-Nordheim field emission theory for nonplanar metal emitters, Appl. Phys. Lett. **59**, 1644 (1991).
[13] P. H. Cutler, J. He, J. Miller, N. M. Miskovsky, B. Weiss, and T. E. Sullivan, Theory of electron emission in high fields from atomically sharp emitters: Validity of the Fowler-Nordheim equation, Prog. Surf. Sci. **42**, 169 (1993).
[14] G. N. Fursey, L. M. Baskin, D. V. Glazanov, A. O. Yevgen'ev, A. V. Kotcheryzhenkov, and S. A. Polezhaev, Specific features of field emission from submicron cathode surface areas at high current densities, J. Vac. Sci. Technol. B **16**, 232 (1998).
[15] S. A. Guerrera, L. F. Velásquez-García, and A. I. Akinwande, Scaling of high-aspect-ratio current limiters for the individual ballasting of large arrays of field emitters, IEEE Trans. Electron Devices **59**, 2524 (2012).
[16] D. A. Zanin, H. Cabrera, L. G. De Pietro, M. Pikulski, M. Goldmann, U. Ramsperger, D. Pescia, and J. P. Xanthakis, Fundamental aspects of near-field emission scanning electron microscopy, Adv. Imaging Electron Phys. **170**, 227 (2012).
[17] M. T. Cole, R. J. Parmee, A. Kumar, C. M. Collins, M. H. Kang, J. Xiao, C. Cepek, X. Yuanc, and W. I. Milne, Conjugated polyelectrolyte nano field emission adlayers, Nanoscale Horiz. **1**, 304 (2016).
[18] P. D. Joshi, D. S. Joag, D. J. Late, and I. S. Mulla, Nonlinear Fowler-Nordheim behavior of a single SnO_2 nanowire, J. Vac. Sci. Technol. B **35**, 02C105 (2017).
[19] C. J. Edgcombe, Development of Fowler-Nordheim theory for a spherical field emitter, Phys. Rev. B **72**, 045420 (2005).
[20] A. Kyritsakis and J. P. Xanthakis, Derivation of a generalized Fowler-Nordheim equation for nanoscopic field-emitters, Proc. R. Soc. A **471**, 20140811 (2015).
[21] A. Kyritsakis and J. P. Xanthakis, Extension of the general thermal field equation for nanosized emitters, J. Appl. Phys. **119**, 045303 (2016).
[22] R. Gomer, On the mechanism of liquid metal electron and ion sources, Appl. Phys. A **19**, 365 (1979).
[23] U. Mizutani, *Introduction to the Electron Theory of Metals* (Cambridge University Press, Cambridge, England, 2001).
[24] R. G. Forbes, Simple derivation of the formula for Sommerfeld supply density used in electron-emission physics and limitations on its use, J. Vac. Sci. Technol. B **28**, 1326 (2010).
[25] Y. S. Ang and L. K. Ang, Current-Temperature Scaling for a Schottky Interface with Nonparabolic Energy Dispersion, Phys. Rev. Applied **6**, 034013 (2016).
[26] S.-J. Liang and L. K. Ang, Electron Thermionic Emission from Graphene and a Thermionic Energy Converter, Phys. Rev. Applied **3**, 014002 (2015).
[27] X.-Z. Qin, W.-L. Wang, N.-S. Xu, Z.-B. Li, and R. G. Forbes, Analytical treatment of cold field electron emission from a nanowall emitter, including quantum confinement effects, Proc. R. Soc. A **467**, 1029 (2011).
[28] A. A. Patterson and A. I. Akinwande, Elementary framework for cold field emission from quantum-confined, nonplanar emitters, J. Appl. Phys. **117**, 174311 (2015).
[29] S. C. Miller, Jr. and R. H. Good, Jr., A WKB-type approximation to the Schrödinger equation, Phys. Rev. **91**, 174 (1953).
[30] E. C. Kemble, *The Fundamental Principles of Quantum Mechanics* (McGraw-Hill, New York, 1937).
[31] K. L. Jensen, D. A. Shiffler, J. R. Harris, I. M. Rittersdorf, and J. J. Petillo, 2D/3D image charge for modeling field emission, J. Vac. Sci. Technol. B **35**, 02C101 (2017).
[32] D. J. Griffiths, *Introduction to Electrodynamics*, 3rd ed. (Prentice-Hall, New Jersey, 1999).
[33] R. G. Forbes, Simple good approximations for the special elliptic functions in standard Fowler-Nordheim tunneling theory for a Schottky-Nordheim barrier, Appl. Phys. Lett. **89**, 113122 (2006).
[34] J. H. B. Deane and R. G. Forbes, The formal derivation of an exact series expansion for the principal Schottky-Nordheim barrier function v, using the Gauss hypergeometric differential equation, J. Phys. A **41**, 395301 (2008).
[35] L. W. Swanson and G. A. Schwind, in *Handbook of Charged Particle Optics*, 2nd ed., edited by J. Orloff (CRC Press, Boca Raton, 2009), Chap. 1, pp. 1–28.
[36] R. G. Forbes, On the need for a tunneling pre-factor in Fowler-Nordheim tunneling theory, J. Appl. Phys. **103**, 114911 (2008).
[37] R. G. Forbes, A. Fischer, and M. S. Mousa, Improved approach to Fowler-Nordheim plot analysis, J. Vac. Sci. Technol. B **31**, 02B103 (2013).
[38] A. S. Bahm, G. A. Schwind, and L. W. Swanson, Range of validity of field emission equations, J. Vac. Sci. Technol. B **26**, 2080 (2008).
[39] R. D. Young, Theoretical total-energy distribution of field-emitted electrons, Phys. Rev. **113**, 110 (1959).
[40] J. M. Bonard, K. A. Dean, B. F. Coll, and C. Klinke, Field Emission of Individual Carbon Nanotubes in the Scanning Electron Microscope, Phys. Rev. Lett. **89**, 197602 (2002).
[41] J. S. Gilbert, S. J. Lane, R. S. J. Sparks, and T. Koyaguchi, Charge measurements on particle fallout from a volcanic plume, Nature (London) **349**, 598 (1991).
[42] M. Coppins, Electrostatic Breakup in a Misty Plasma, Phys. Rev. Lett. **104**, 065003 (2010).

[43] Y. B. Zhu and L. K. Ang, Space charge limited current emission for a sharp tip, Phys. Plasmas **22**, 052106 (2015).

[44] K. L. Jensen, D. A. Shiffler, I. M. Rittersdorf, J. L. Lebowitz, J. R. Harris, Y. Y. Lau, J. J. Petillo, W. Tang, and J. W. Luginsland, Discrete space charge affected field emission: Flat and hemisphere emitters, J. Appl. Phys. **117**, 194902 (2015).

[45] K.-U. Riemann, The Bohm criterion and sheath formation, J. Phys. D **24**, 493 (1991).